PROCEEDINGS A

royalsocietypublishing.org/journal/rspa

Research

Cite this article: Calvelage CM, Wu J, Colli L, Lin Y-A, Zheng Y. 2024 Linking deep-time subduction history to modern day expressions of dynamic topography. *Proc. R. Soc. A* **480**: 20240254.
https://doi.org/10.1098/rspa.2024.0254

Received: 7 April 2024
Accepted: 23 August 2024

Subject Category:
Earth science

Subject Areas:
geophysics

Keywords:
dynamic topography, Pacific plate tectonics, mantle convection

Author for correspondence:
Jonny Wu
e-mail: jonnywu@arizona.edu

One contribution to a special feature 'Foundations of Operational Geodynamics' organized by guest editors Hans-Peter Bunge, Huw Davies and Sergei Lebedev.

Electronic supplementary material is available online at https://doi.org/10.6084/m9.figshare.c.7458425.

THE ROYAL SOCIETY PUBLISHING

Linking deep-time subduction history to modern day expressions of dynamic topography

C. M. Calvelage[1], Jonny Wu[1,2], Lorenzo Colli[1,3], Yi-An Lin[1,4] and Yingcai Zheng[1]

[1]Department of Earth and Atmospheric Sciences, University of Houston, Houston, TX, USA
[2]Department of Geosciences, University of Arizona, Tucson, AZ, USA
[3]BlueThink, Milan, Italy
[4]CenterPoint Energy, Houston, TX, USA

CMC, 0009-0005-9807-4255; JW, 0000-0001-5530-005X

Dynamic topography refers to vertical deflections of Earth's surface from viscous flow within the mantle. Here we investigate how past subduction history affects present dynamic topography. We assimilate two plate reconstructions into TERRA forward mantle convection models to calculate past mantle states and predict Earth's present dynamic topography; a comparison is made with a database of observed oceanic residual topography. The two assimilated plate reconstructions 'Earthbyte' and 'Tomopac' show divergent subduction histories across an extensive deep-time interval within Pacific-Panthalassa. We find that introducing an alternative subduction history perturbs our modelled present-day dynamic topography on the same order as the choice of radial viscosity. Additional circum-Pacific intra-oceanic subduction in Tomopac consistently produces higher correlations to the geoid (more than 20% improvement). At spherical harmonic degrees 1–40, dynamic topography models with intra-oceanic subduction produce universally higher correlations with observations and improve fit by up to 37%. In northeast Asia, Tomopac models show higher correlations (0.46 versus 0.18) to observed residual topography and more accurately predict approximately 1 km of dynamic subsidence within the Philippine Sea plate. We demonstrate that regional deep-time changes in subduction history have widespread impacts on the spatial distribution

and magnitude of present-day dynamic topography. Specifically, we find that local changes to plate motion histories can induce dynamic topography changes in faraway regions located thousands of kilometres away. Our results affirm that present-day residual topography observations provide a powerful, additional constraint for reconstructing ancient subduction histories.

1. Introduction

Earth's surface topography is the product of both isostasy and mantle convection [1,2]. The portion of Earth's topography that is driven by mantle convection, known as dynamic topography, refers to the change in topography that arises from viscous flow within Earth's mantle (figure 1) [4–6]. Dynamic changes to Earth's topography are fundamental towards understanding phenomena that include global sea level changes [7,8], the stability of ice sheets [9], sediment transport [10,11] and biodiversity [11]. Here we focus on dynamic topography within Earth's oceans, which is more straightforward to interpret because the oceanic lithosphere contains fewer heterogeneities than the continental lithosphere. Also, seafloor bathymetry change is primarily controlled by the cooling of the oceanic crust as it moves away from mid-ocean ridge spreading centres [12]. Thus, deviations from the expected seafloor depth can be attributed to dynamic topography after correcting for sedimentary and crustal loading (figure 1).

Present-day dynamic topography (e.g. figure 2*a–c*) is sensitive to past mantle flow states [4,14–17]. Previous studies have modelled dynamic topography using increasingly refined models of mantle flow that assimilate plate kinematic reconstructions in million-year increments [2,16,18]. The assimilated plate reconstruction and its associated subduction history should have considerable effects on dynamic topography because subduction plays an important role in mantle convection [19,20]. However, the role of subduction history on dynamic topography has not been fully investigated. Here, we examine the effect of subduction history on dynamic topography using forward global geodynamic models that assimilate two differing plate reconstructions within a large region (Pacific-Panthalassa) across a protracted time interval from the Jurassic to early Cenozoic (figure 3); variable radial viscosities are also considered. The plate tectonic history of the Pacific-Panthalassa represents an area of uncertainty reaching up to 65% of Earth's oceans (white regions in figure 3) and is challenging to reconstruct because much of the seafloor has been recycled by subduction. This large uncertainty makes the Pacific-Panthalassa region an excellent testbed for examining the effects of subduction history within present oceanic regions, which is now densely sampled (see figure 8) [6].

(a) A rapidly improving oceanic dynamic topography database

Previous studies have characterized the magnitude and spatial distribution of present-day oceanic dynamic topography [4–6,17]. Since the original analysis of Menard [17], the main challenge in producing estimates of dynamic topography has been obtaining accurate measurements of density and sedimentary and crustal thickness [3,5,6]. To address this limitation, Winterbourne *et al.* [3] and Hoggard *et al.* [4,5] implemented the use of seismic reflection surveys and seismic refraction experiments. The recent database published by Holdt *et al.* [6] considerably expands these methods and uses 1411 multi-channel and 5444 single-channel seismic reflection profiles, together with 323 modern seismic wide-angle experiments and 423 vintage seismic refraction experiments. These new measurements give good coverage of the oceanic domain and provide 10 874 residual depth estimates for comparison with model predictions [6], which is a more than 300% increase in coverage over previous studies [5]. These

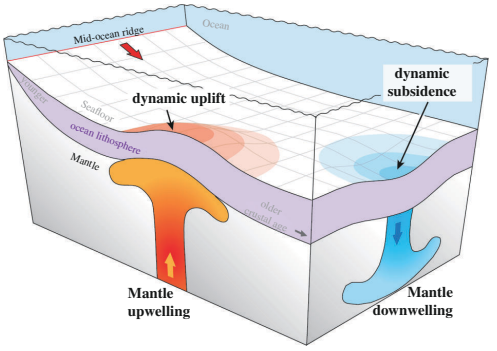

Figure 1. A graphic representation showing dynamic uplift and dynamic subsidence within an oceanic region from viscous stresses due to mantle upwelling and downwelling, known as dynamic topography (modified from [3]; K Czarnota 2022, personal communication). The seafloor deepens at a known rate as the ocean lithosphere cools and becomes older, shown here by its relative distance from the mid-ocean ridge. Dynamic topography is inferred in regions where the seafloor is anomalously shallower or deeper relative to the expected seafloor depth.

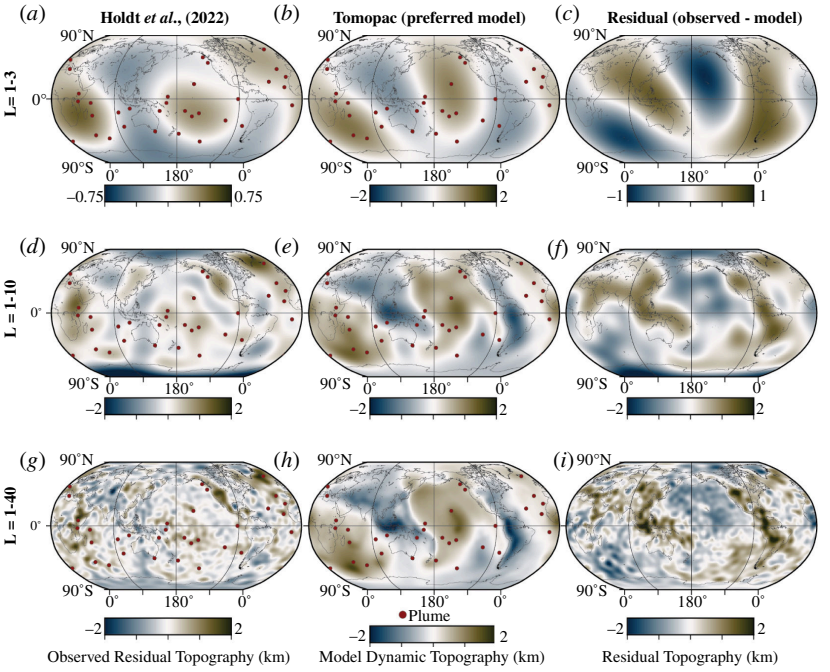

Figure 2. Maps of observed oceanic dynamic topography from Holdt *et al.* [6] plotted at spherical harmonic summations of 1–3, 1–10 and 1–40, respectively (*a,d,g*).The second column (*b,e,h*)shows predicted dynamic topography from the Tomopac model using the preferred radial viscosity profile visc06 at increasing spherical harmonic summations. The third column (*c,f,i*)is the residual between the observed residual topography and model dynamic topography. Red dots show plumes from a global catalogue [13]. A similar plot for the Earthbyte model is shown in the electronic supplementary material, figure S9.

new observations constrain the magnitudes of oceanic dynamic topography to approximately ±2 km and spatial length scales of the order of approximately 1500 km or a spherical harmonic degree of 40 (figure 2*c*) [6].

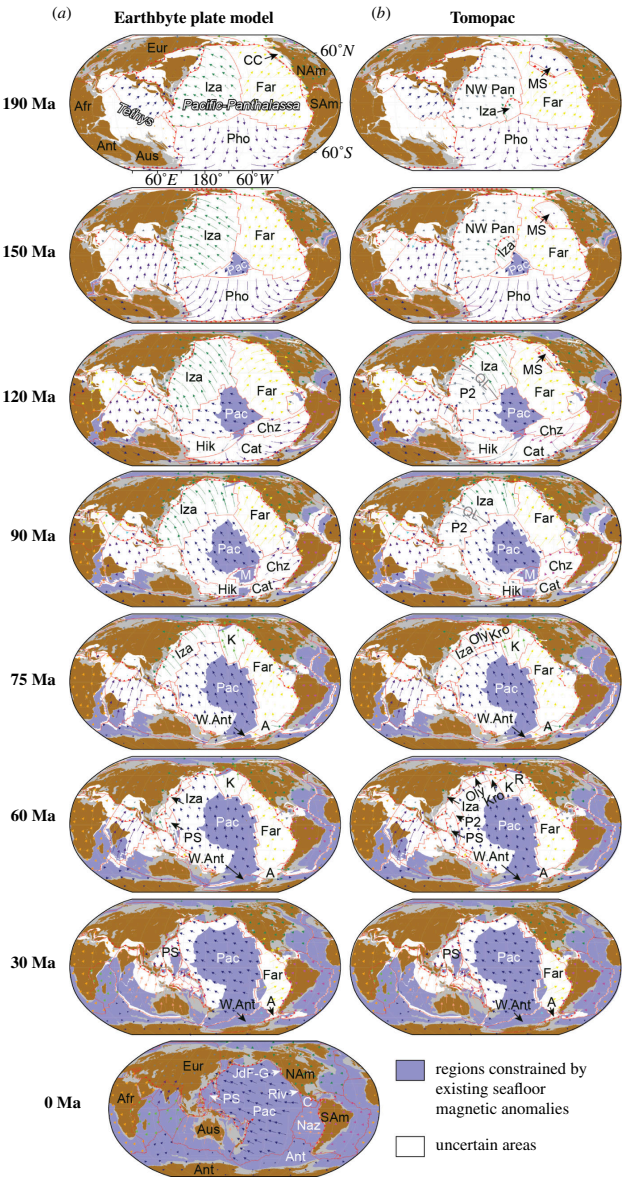

Figure 3. Maps showing two input plate tectonic reconstruction models from 190 Ma to present: (*a*) Earthbyte reference [21] and (*b*) Tomopac [22]. Plates and plate boundaries relevant to the Pacific-Panthalassa realm are highlighted. Abbreviations —A: Aluk; Afr: Africa; Ant: Antarctica; Aus: Australia; Cat: Catequil; CC: Cache Creek; Chz: Chazca; Eur: Eurasia; Far: Farallon; Hik: Hikurangi; Iza: Izanagi; JdF-G: Juan de Fuca-Gorda; K: Kula; Kro: Kronotsky; M: Manihiki; MS: Marginal Sea; NAm: North America; NW Pan: NW Panthalassic plate; Oly: Olytorsky; P2: NW Panthalassic plate 2; Pho: Phoenix; PS: Philippine Sea; QL: Qingdao line divergent-transform; R: Resurrection; Riv: Riviera; SAm: South America; W.Ant: Western Antarctic.

(b) Predicting dynamic topography

Previous studies have modelled dynamic topography in an effort to examine Earth's parameters such as density and viscosity [14,23,24]. However, the impact of subduction history (i.e. altering the plate reconstruction) on dynamic topography has been scarcely considered. Subduction histories are not easily reconstructed because oceanic lithosphere and associated geological information is lost from the Earth's surface and recycled into the mantle during the process of subduction. Moreover, even when multiple subduction histories are proposed,

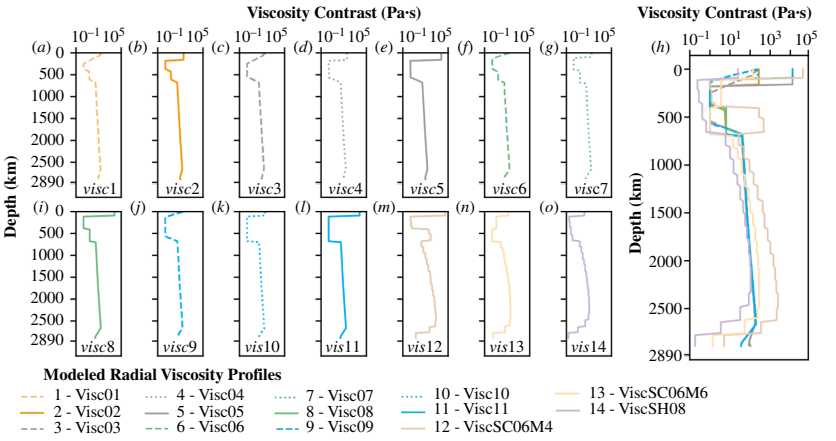

Figure 4. Depth versus viscosity contrast plots of 14 radial viscosity profiles used in the synthetic geoid and True Polar Wander (TPW) calculations. References: visc 01–visc 11 (*a–k*) are from Lin *et al.* [16] and are slight permutations of the viscosity profile used in their mantle convection models; (*l*)visc12 SC06M4 is model 4 of Steinberger & Calderwood [26]; (*m*) visc13 SC06M6 is model 6 of Steinberger & Calderwood [26]; (*n*) visc14 SH08 is from Steinberger & Holme [24]. (*o*) All profiles plotted together. See the electronic supplementary material, Data for digital files for all 14 radial viscosity files.

only a few studies have undertaken the significant challenges in producing alternative but comparable plate motion models that are suitable for mantle convection modelling (i.e. global, fully kinematic, topologically closed and using similar mantle references and plate circuits) [15,16,19,25].

Here, we compare the predicted oceanic dynamic topography from two global, topologically closed plate tectonic reconstructions using similar mantle references and assimilate these into TERRA mantle convection models. The two plate models are (figure 3): (i) a widely used global plate model that we call Earthbyte ('corrected R' Matthews *et al.* [21]) and (ii) Tomopac, a newly developed global plate tectonic model that attempts to enhance subduction history within the circum-Pacific regions using structurally restored slabs from mantle seismic tomography [22]. The time series of geodynamically modelled mantle states is used to calculate model dynamic topography from viscous stresses induced by mantle convection. Viscosity is an important consideration [2] and we consider 14 viscosity-depth profiles (figure 4). We test the modelled dynamic topography by comparing them with published oceanic residual depth observations [6] (figure 2*a–c*) and discuss the impact of subduction histories on regional dynamic topography in NE Asia, where subduction histories are vigorously debated.

2. Methods

(a) Global mantle convection models

Following the workflow of Calvelage *et al.* (this issue) [27] and Lin *et al.* [15,16], we use the finite element code TERRA [28] to solve the equations for the conservation of mass, momentum and energy in the truncated anelastic liquid approximation for a compressible fluid with an infinite Prandtl number in a spherical shell [29] with an Earth-like radius. The models have 128 layers with a total of approximately 80 million grid points and an icosahedral grid spacing of approximately 25 km. The velocities at the outer surface are set by the plate reconstruction of interest (reviewed in 2b) and scaled by a factor of 2.1 to avoid forced convection. The core mantle boundary (CMB) is set to free slip. Temperatures are kept constant at the surface and at the CMB while mantle temperatures are determined self-consistently by the governing

equations. Compositionally, the mantle is treated as homogeneous with bottom and internal heating. The Newtonian viscosity depends on temperature and depth as

$$\eta(d, T) = \eta_0 A(d)\, e^{V^* \frac{d}{r_E - r_{CMB}} - E^* \frac{T - T_s}{T_{CMB} - T_s}}, \tag{2.1}$$

where η_0 is the reference viscosity, $A(d)$ is the radial prefactor to impose a low viscosity asthenosphere, $V^* = 2.996$ is the activation volume, which determines the sensitivity of viscosity to depth and $E^* = 4.605$ is the activation energy, which determines the sensitivity of viscosity to temperature. The reference viscosity is 10^{22} Pa·s with lateral variations limited to the range of 10^{-2} to 10^2 Pa·s. The rheology described above results in double-sided subduction because we do not impose weak plate boundaries or a prescribed slab thermal structure.

The Gruneisen parameter, which is used to calculate the depth-dependent density of the mantle by integrating the self-compression equation, is set to 1.1. The mantle temperature was converted to density using

$$\rho(x) = \rho_0(1 - \alpha \Delta T(x)), \tag{2.2}$$

where α is the thermal expansivity, ρ_0 is the reference equilibrium density and ΔT is the temperature difference [30]. A global cross section characterizing the mantle circulation model results is shown in the electronic supplementary material, figure S1.

(b) Input plate reconstructions

Global plate reconstructions provide the time-dependent surface boundary velocity conditions for our global mantle convection models. Subduction histories from plate reconstructions play an important role in altering mantle convection [18,19]; therefore, it is reasonable to expect that alternative plate reconstruction histories will produce a contrasted mantle structure that in turn produces different predicted dynamic topography. Following Calvelage *et al.* (this issue) [27] we assimilate two different plate reconstructions into mantle convection models to test the effects of implemented deep-time subduction history on predicted dynamic topography (figure 3). The first plate reconstruction we call 'Earthbyte' is the Matthews *et al.* [21] 'corrected R' global plate model (figure 3*a*). The second plate reconstruction we call 'Tomopac' is a global plate tectonic model of the circum-Pacific using structurally restored slabs from mantle seismic tomography and other constraints [22] (figure 3*b*). Plate reconstruction files that describe Tomopac [22] at all timesteps for open source GPlates software are publicly accessible through an online data repository [31]. The Tomopac plate reconstruction is recently developed [22] and not yet fully described in the literature. Therefore, we describe the pertinent details of Tomopac below.

Tomopac uses the 'corrected R' [21] plate model as a base (i.e. similar mantle reference frames and global plate circuits). Tomopac attempts to enhance plate tectonic histories between the time periods 190 and 50 Ma within uncertain regions of the circum-Pacific, which are sizeable (white areas in figure 3). The Tomopac [22] and Earthbyte [21] plate models are essentially identical after 50 Ma (figure 3). The largest differences between the Earthbyte and Tomopac plate models occur within the north and central Pacific-Panthalassa near NE Asia (figure 3). From the birth of the Pacific plate at approximately 190 Ma until an apparent Izanagi-Pacific plate reorganization at approximately 145 Ma based on approximately 24° clockwise rotation of the Izanagi plate relative to the Pacific at chron M21 [32], Tomopac implements intra-oceanic subduction of a remnant 'NW Panthalassa' plate ('NW Pan' in figure 3*b*) under the growing Izanagi plate following the preferred plate reconstruction of Lin *et al.* [16]. Intra-oceanic subduction within the NW Pacific during this period is supported by accreted intra-oceanic arc crust of Jurassic to earliest Cretaceous ages within the Oku-Niikappu subduction complex, Hokkaido, Japan [33]. After the approximately 145 Ma Izanagi–Pacific plate reorganization, Tomopac implements a 'Qingdao line' divergent transform plate boundary ('QL' in figure 3*b*) that segments the NW Pacific subduction domains following

tomographic slab reconstructions and NE Asia continental arc magmatic histories [34]. From 85 Ma to the early Cenozoic, Tomopac implements the Kronotsky and Olyutorsky intra-oceanic subduction zones (figure 3*b*) following Vaes *et al.* [35]; intra-oceanic subduction within the North Pacific during this period is consistent with tomography, paleomagnetism and the geological histories of accreted oceanic terranes [35,36].

In western North America, Tomopac implements a long-lived intra-oceanic subduction zone related to the now-accreted Wrangellia Composite Terrane (WCT) and subduction of an unnamed marginal sea plate along western North America that terminates with WCT-North America collision at approximately 100 Ma [37]. By contrast, Matthews *et al.* [21] implement a similar intra-oceanic subduction zone and associated 'Cache Creek' marginal sea ('CC' in figure 3*a*) that collided with North America earlier at 180 Ma (figure 3*a*). In South America, Tomopac is broadly similar to Matthews *et al.* [21] but Tomopac implements a brief stalling of oceanic subduction under western South America from 100 to 85 Ma (figure 3*b*) based on tomographic lower mantle slabs, arc magmatism and Andean shortening histories [38]. To implement the plate reconstructions into TERRA global mantle convection models, we follow the modelling approach of Lin *et al.* [16]. We start from 410 Ma to generate an initial convective state; the alternative plate models are assimilated for 160 Ma (Earthbyte) or 190 Ma (Tomopac) when the plate reconstructions begin to kinematically differ from each other (figure 3).

Our comparison of dynamic topography from two significantly contrasting plate reconstructions across a protracted time period (>100 Myrs) is novel because most mantle convection models primarily assimilate one common family of plate reconstructions for surface boundary conditions [19,39,40]; this class of popular plate reconstructions are represented by our Earthbyte reference model [21]. Furthermore, because the Earthbyte and Tomopac subduction histories are identical from 50 to 0 Ma, we expect most of the differences in modelled mantle structure to be at deeper mantle depths. This allows us to probe the sensitivity predictions of present-day dynamic topography to deeper mantle structures that presumably are affected by the deeper time subduction history.

(c) Geoid and dynamic topography computation

The geoid is the equipotential surface of the gravity field that is equivalent to the mean sea level and includes significant contributions from density anomalies within the mantle and density anomalies induced by dynamic surface and CMB topography [41]. From the mantle convection models described above, we calculate a synthetic geoid for each model timestep following Thoraval & Richards [42] based on the semi-analytical solutions from an expansion in spherical harmonics (electronic supplementary material, figures S2 and S3). We assume the reference density profile of AK-135 [43], water loaded topography and a free slip condition on the CMB and surface. To compensate for unrealistic thermal boundary layers, the isochemical nature of TERRA and lower Rayleigh numbers with respect to the observable Earth, we choose to disregard all density anomalies shallower than 350 km (i.e. depth cut-off) for our geoid calculation. We use a depth cut-off due to its straightforward implementation even though more calibrated approaches that consider boundary layer compositional changes and anelasticity effects for thermomechanical upper mantle structure are available [44], which are discussed later.

A depth cut-off has been implemented by numerous dynamic topography studies [2,16,45,46] to mitigate unrealistically large magnitudes (> ± 2 km) of dynamic topography relative to observations (figure 2*a–c*) [6]. For this study, we find that a 350 km depth cut-off produces a more realistic range of dynamic topography magnitudes (=± 2 km) even though the magnitudes are still overpredicted at spherical harmonic degrees 1 to 3 (figure 2*a*,*d*). By comparison, shallower depth cut-offs (200 or 150 km) produce excessively high dynamic topography magnitudes (electronic supplementary material, figure S12). Our choice of a 350 km cut-off depth reduces the spectral power in our modelled dynamic topography compared

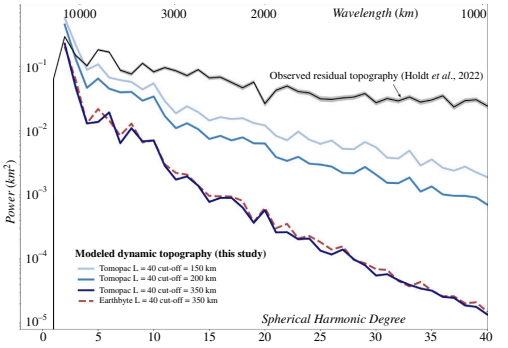

Figure 5. Plot of the power versus spherical harmonic degree for residual topography observations of Holdt *et al.* [6] and the dynamic topography models from this study using preferred radial viscosity profile visc06 (figure 4). The Holdt *et al.* [6] power spectrum is plotted in black with the uncertainty shaded in grey. The model power spectra are shown with various depth cut-offs (i.e. the depth that the uppermost mantle was truncated in the geodynamic model). Shallower depth cut-offs yield higher power at higher spherical harmonic degrees (i.e. degrees 20 to 40) that produce a more similar slope to the observational data (i.e. they are sub-parallel). Mantle models using the Tomopac and Earthbyte plate reconstructions show nearly identical power spectra.

with shallower cut-off depths (figure 5). This trade-off likely occurs because our models preclude asthenospheric heterogeneities that might account for shorter wavelength dynamic topography [4,5,44]. Therefore, we expect that our models will not accurately reproduce Earth's observed residual topography at higher wavelengths (spherical harmonic degrees > 10) similar to previous studies [2]. Nonetheless, we will compare our models against observations at a variety of spherical harmonic degree summations (e.g. figure 2) and further discuss these limitations in §4.

The geoid can be expressed as the product of the spherical harmonic coefficients of the geoid, G_{lm}, and the spherical harmonic function, Y_{lm}, a function of latitude and longitude summed over the spherical harmonic degrees and orders, l and m, respectively:

$$G(\theta,\varphi) = \sum_{l=0}^{\infty}\sum_{m=-l}^{\infty}\left(G^{S}_{lm}Y^{S}_{lm}(\theta,\varphi)\right) + \left(G^{C}_{lm}Y^{C}_{lm}(\theta,\varphi)\right). \tag{2.3}$$

Density contrasts within the Earth can be expressed similarly, with the spherical harmonic coefficients replaced by those for density anomalies as a function of the Earth's radius:

$$\delta\rho(r,\theta,\varphi) = \sum_{l=0}^{\infty}\sum_{m=-l}^{\infty}\left(\delta\rho^{S}_{lm}(r)Y^{S}_{lm}(\theta,\varphi)\right) + \left(\delta\rho^{C}_{lm}(r)Y^{C}_{lm}(\theta,\varphi)\right). \tag{2.4}$$

The spherical harmonic function, along with its associated coefficients, are separated into sine and cosine terms below:

$$Y^{S}_{lm}(\theta,\varphi) = (-1)^{m}\sqrt{2-\delta_{m0}}\sqrt{\frac{(2l+1)(l-m)!}{(l+m)!}}P_{lm}(\cos\theta)\sin(m\varphi), \tag{2.5}$$

$$Y^{C}_{lm}(\theta,\varphi) = (-1)^{m}\sqrt{2-\delta_{m0}}\sqrt{\frac{(2l+1)(l-m)!}{(l+m)!}}P_{lm}(\cos\theta)\cos(m\varphi), \tag{2.6}$$

where P_{lm} are Legendre polynomials. The solution can then be expressed in spherical harmonic space with the following relationship between the spherical harmonic coefficients of the geoid and those of the density anomalies:

$$G_{lm} = \int_{CMB}^{Surf.} \delta\rho_{lm}(r)\, K_{l}(r)\, dr\,. \tag{2.7}$$

The kernels, K_l, express the relative magnitude that a density contrast at a given depth and wavelength contributes to the dynamic topography and the geoid. Kernels are computed using the propagator matrix technique [41].

Like the geoid, we can calculate the dynamic topography using the propagator matrix technique of Richards & Hager [41]. We solve via an expansion in spherical harmonics using sensitivity kernels, which can be regarded as impulse response functions that relate dynamic topography to a density anomaly of a given wavelength and depth, expressed here as radius r. As such, the dynamic topography can be expressed as

$$\delta h_{lm} = \int_{R_{cmb}}^{R_{surf.}} \delta\rho_{lm}(r)\, K_l(r)\, dr, \tag{2.8}$$

where δh_{lm} is the dynamic topography at spherical harmonic degree l and order m. $\delta\rho_{lm}$ is the density anomaly at spherical harmonic degree l and order m. $K_l(r)$ are the sensitivity kernels. The final values of dynamic topography are obtained by a resummation of the calculated spherical harmonic coefficients at degrees 1–3, 1–10 and 1–40. Previous studies have indicated that dynamic topography is sensitive to Earth's radial viscosity profile [47]. To account for variability produced by changes in radial viscosity, we implement 14 different radial viscosity profiles that are designed to probe the mantle viscosity parameter space (figure 4; see the electronic supplementary material, Data for digital files of the radial viscosity profiles).

3. Results

(a) Effects of subduction history on predicted dynamic topography

(i) Comparison between modelled geoid and observed geoid

The final state of the mantle convection models that assimilated the Earthbyte and Tomopac plate reconstructions (figure 3) are shown in the electronic supplementary material, figures S2 and S3, respectively. As expected, our models show differences in lower mantle structures under the present northwest Pacific and the North and South American Cordillera, where the Earthbyte and Tomopac plate models show different subduction histories between the Jurassic to early Cenozoic (electronic supplementary material, figure S8). We compute synthetic geoids from the modelled present-day mantle structure for our 14 radial viscosity cases and compare them with the observed Earth geoid at various spherical harmonic summations (degrees 1–3, 1–10 and 1–40) (figure 6). Each of our 14 viscosity cases produces unique predictions of dynamic topography because the choice of radial viscosity changes the magnitude of normal stress transferred to the surface. Spatial maps of each degree to 40 geoid can be found in the electronic supplementary material, figures S4–S7.

Our synthetic geoids show correlations of 0.18 to 0.57 to the actual Earth geoid at spherical harmonic degrees 1–3, 1–10 and 1–40 (figure 6). Our range of correlation values is of the order of previous studies that use time-dependent mantle convection models [16,39,48]. The correlations between synthetic and actual geoid at higher spherical harmonic degree summations (e.g. figure 6*b*,*c*) are not dramatically different from the lower wavelength degree 1–3 summations (e.g. figure 6*a*), which is not surprising because the Earth's geoid power spectrum shows much higher spectral energy at the longer wavelengths. Synthetic geoids calculated using the Tomopac mantle model produce unequivocally higher geoid correlations than Earthbyte for all 14 tested viscosity profiles and at all spherical harmonic degree summations (figure 6). At all tested spherical harmonic degrees, synthetic geoids from the Tomopac mantle model improve the fit to actual geoid relative to Earthbyte by an average R-value increase of approximately 30%, with a range of improvement between minimum 21% and maximum 61%.

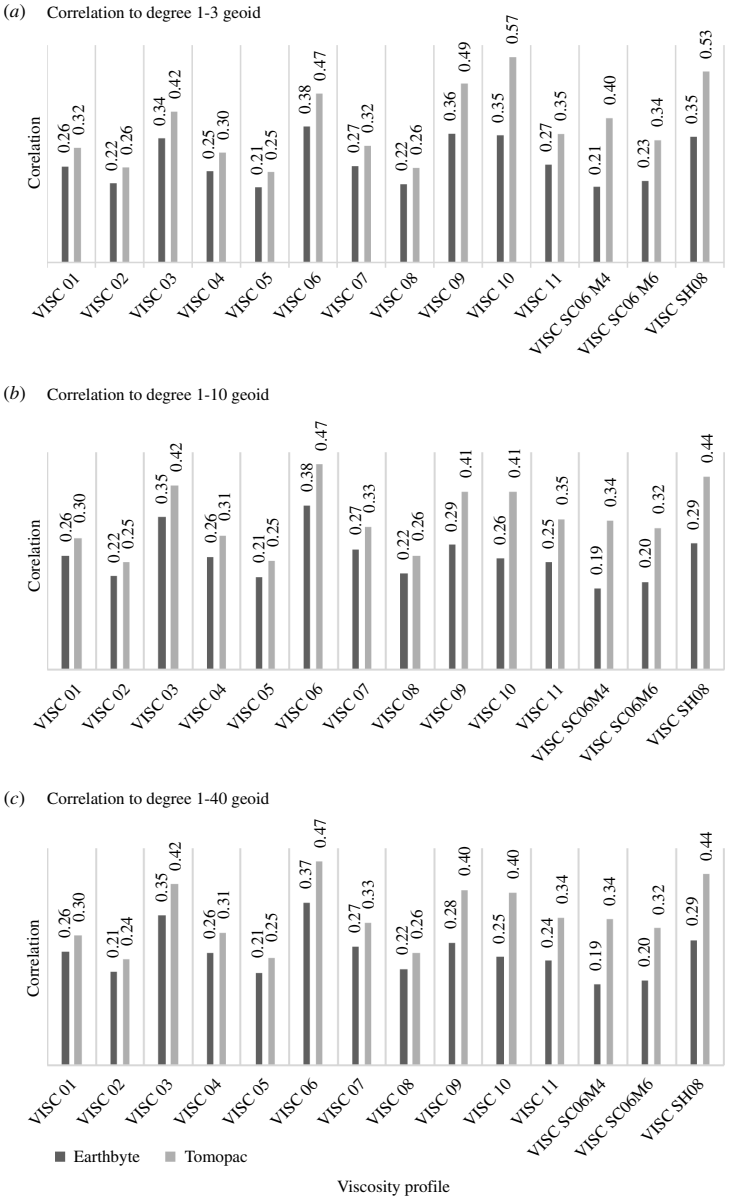

Figure 6. A bar graph of the correlation between the modelled and observed present-day geoid at (*a*) spherical harmonic degree 3, (*b*) spherical harmonic degree 10 and (*c*) spherical harmonic degree 40 (*b*) for the 14 modelled radial viscosity profiles in this study (see figure 4). The numbers above each bar are the Pearson correlation coefficients. The black and grey bars denote synthetic geoids computed from mantle convection models that assimilated the Earthbyte and Tomopac plate reconstructions, respectively.

The 14 radial viscosity cases altered the correlation between synthetic and actual geoid by about the same order (approx. 50%) as changes to the subduction history (i.e. Earthbyte or Tomopac) (figure 6). For example, for the spherical harmonic degree 1–10 geoid, the Earthbyte geoids showed correlations between 0.19 and 0.35 between viscosity cases and the Tomopac geoid correlations varied between 0.25 and 0.47 (figure 6*b*). We compute dynamic topography for the five viscosity cases that show the best geoid correlations for both mantle models (electronic supplementary material, figures S10 and S11). For a given mantle model (i.e. Tomopac or Earthbyte), the predicted dynamic topography using the five viscosity profiles

show similar first-order spatial patterns but differ at smaller scales, for example, present western North America (electronic supplementary material, figures S10 and S11).

(ii) Comparison between predicted dynamic topography versus observed residual topography

Comparisons between our predicted dynamic topography and observed oceanic residual topography from Holdt *et al*. [6] will vary according to the spherical harmonic degree summation that is used for the comparison (figure 2; electronic supplementary material, figure S9). Holdt *et al*. [6] show that most dynamic topography can be described by a spherical harmonic summation of up to degree 40 (figure 2*c*). Our mantle models do not appear to contain adequate signals at shorter wavelengths (i.e. up to spherical harmonic degree 40) for a full comparison with Holdt *et al.* [6] (figure 2*g–i*) but can account for longer wavelength (up to degree 3) and possibly intermediate wavelength (up to degree 10) dynamic topography signals (figure 2*a–h*). Here we choose to compute spherical harmonic summations up to degree 40 for our modelled dynamic topography to facilitate direct spatial comparisons with the residual topography spot measurements of Holdt *et al*. [6] (figure 7*a*). A caveat is that our models may not contain the full power spectrum of the observations, which will create additional misfits at the shorter wavelengths (i.e. degrees 1–40). Thus, we also provide scatter plot comparisons at other wavelengths (figure 7*b–g*).

Comparison of our modelled dynamic topography with observed residual topography at spherical harmonic degrees 1–40 shows correlations of the order of approximately 0.20. The Tomopac modelled dynamic topography shows higher correlations (0.24 to 0.27) to observed residual topography compared with Earthbyte (0.15 to 0.20) across all 14 radial viscosity profiles (figure 7*a*), similar to our geoid results (figure 6). At longer wavelengths (i.e. spherical harmonic degrees 3 and 10) absolute correlations between model and predicted dynamic topography improve towards approximately 0.50 and the Tomopac and Earthbyte subduction histories produce similar correlations (figure 7*b,e*). Thus, it seems the effects of subduction history (i.e. Earthbyte and Tomopac) are more apparent in our modelled dynamic topography at shorter wavelengths (i.e. spherical harmonic degrees ≥10). For all 14 radial viscosity cases, visc06 (figure 4*f*) shows the highest correlation (0.47) to the present-day Earth geoid at all spherical harmonic degree summations for Earthbyte (figure 6). Visc06 also shows the highest correlations at 1–10 and 1–40 degree summations for Tomopac and also shows a favourable correlation at degrees 1–3 (figure 6). Therefore, our dynamic topography models using the Visc06 viscosity profile are considered our preferred cases and will be used for comparison against observations in §3a(iii).

(iii) Geographic differences in predicted dynamic topography

We examine the spatial difference between our modelled dynamic topography from the Tomopac and Earthbyte mantle models using the best fitting viscosity case Visc06 (figure 8*a,b*) by calculating a residual map (figure 8*c*). The largest differences occur in the northwest Pacific near East Asia where the differences in predicted dynamic topography approach 1 km (dashed grey box in figure 8). The differences in predicted dynamic topography near East Asia are not surprising because the Tomopac and Earthbyte plate reconstructions show significant contrasts in this region between 190 and 50 Ma (figure 3). Apart from strong regional deviations in NE Asia, there are changes in predicted dynamic topography that occur on the global scale ranging from North and South America to Europe and Asia of the order of a few hundred metres to 0.5 km, depending upon the region (figure 8*c*). The differences in predicted dynamic topography in areas where identical plate reconstructions were assimilated across the entire mantle modelling time window (i.e. since 410 Ma; figure 3) such as central Eurasia and Arabia (figure 8*c*), highlight the far-reaching effects of regional subduction history on global mantle flow because the mantle is acting as a highly viscous, continuous fluid. In §3b, we analyse

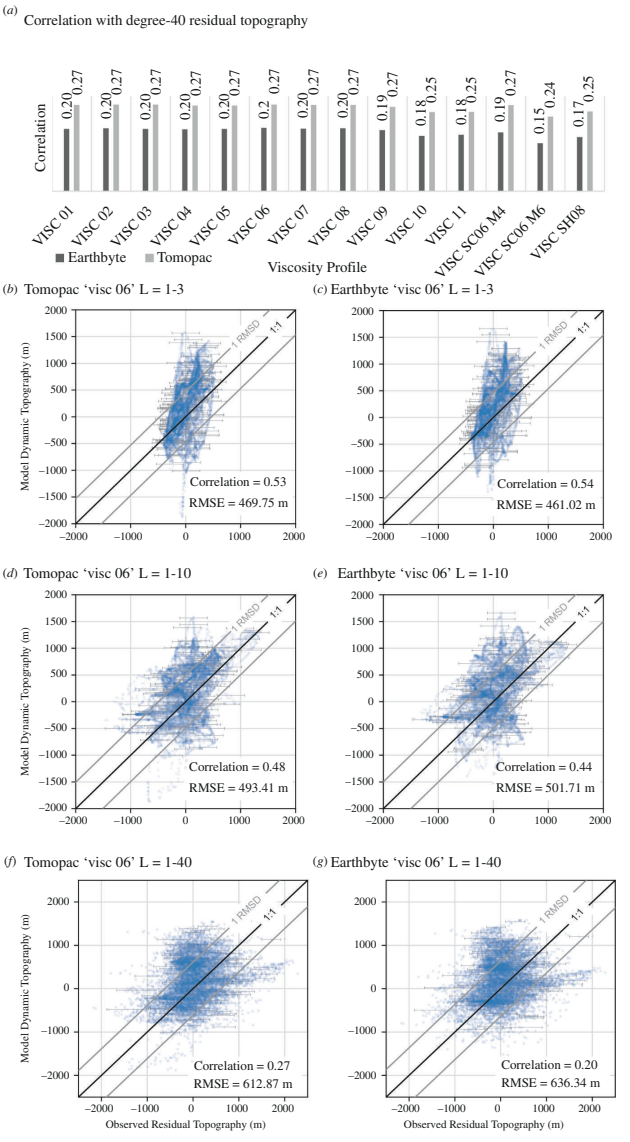

Figure 7. (*a*) Bar graph showing correlations between our modelled dynamic topography and published observed residual topography [6] at spherical harmonic degrees 1 to 40 for each of the 14 radial viscosity profiles in this study (see figure 4). The numbers above each bar are the Pearson correlation coefficients. The black bars are Earthbyte and the grey bars are Tomopac. The bottom rows show scatter plots of modelled dynamic topography against the observed residual topography of Holdt *et al*. [6] for best-fitting viscosity case 06 (i.e. the case with the highest geoid correlation) for (*b–d*) Tomopac and (*e–g*) Earthbyte at spherical harmonic summations 1–3, 1–10 and 1–40. Grey error bars are plotted at every 50 points. RMSE = root mean square error. RMSD = root mean square deviation.

the dynamic topography differences in NE Asia where the predictions between Tomopac and Earthbyte are most disparate (figures 8*c* and 9).

(b) NE Asia case: predicted dynamic topography versus observed residual topography

In NE Asia, the Tomopac and Earthbyte dynamic topography predictions show differences up to 1 km that are testable because Holdt *et al*. [6] show an extensive catalogue of observed residual topography spot measurements (figure 9*a,c*). Here the Tomopac dynamic

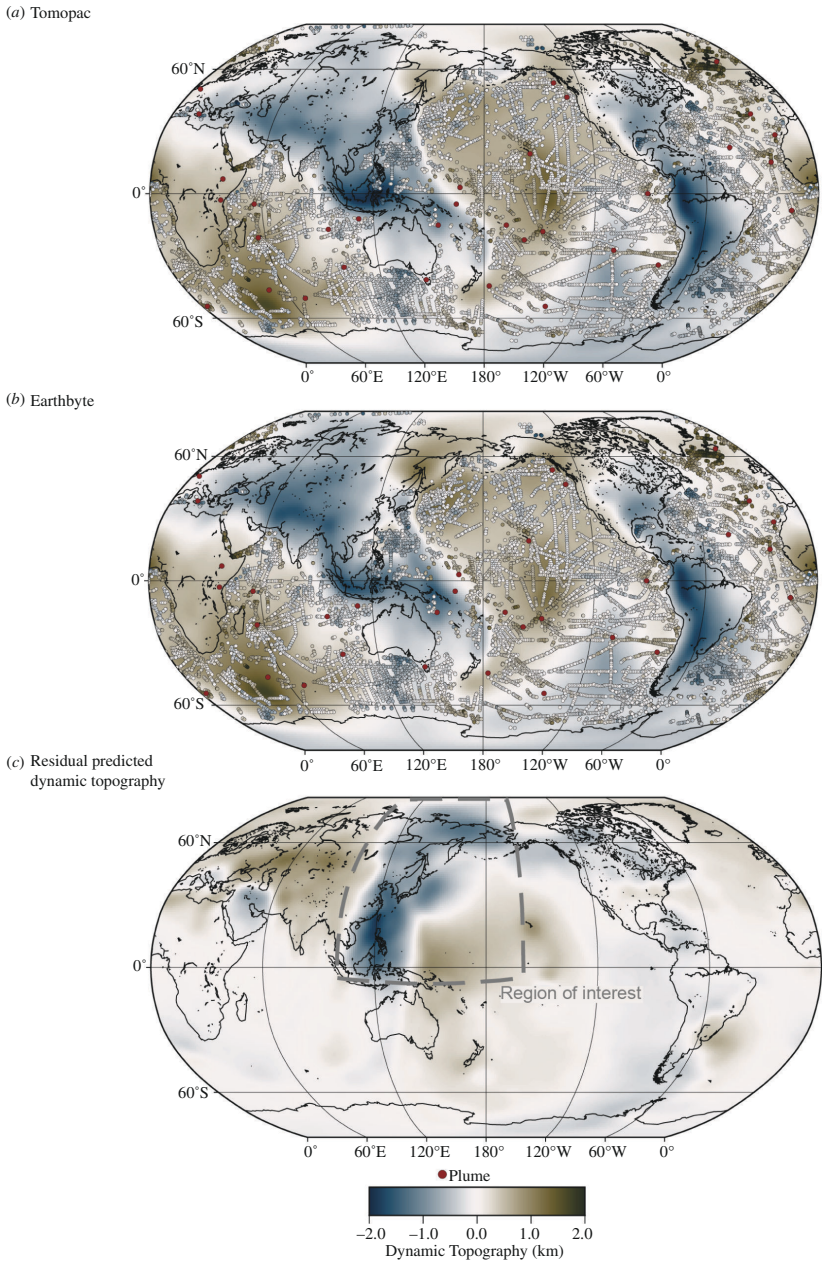

Figure 8. Maps showing modelled dynamic topography from (*a*) Tomopac and (*b*) Earthbyte for preferred viscosity case 06. Background colours show the magnitude of modelled dynamic topography. The points show spot measurements of observed residual topography from Holdt *et al.* [6] that are also colour-coded by dynamic topography magnitude. (*c*) A residual map of (*a*) and (*b*) obtained by subtracting the Earthbyte model predictions from the Tomopac predictions. The residual map highlights the spatial variations in dynamic predictions due to differences in subduction history. The largest differences occur in NE Asia (grey dashed area in (*c*)) where the two plate reconstructions implement significantly different subduction histories; see figure 9 for analysis. Red dots show plumes from the global catalogue of Nolet *et al.* [13].

topography (figure 8*a,b*) significantly outperforms the Earthbyte predictions when compared with observations (correlations of 0.46 compared with 0.18 in figure 9*b,d*). Spatially, Tomopac shows improved predictions of dynamic topography relative to Holdt *et al*. [6] near the Aleutian Islands (180°, 60°N) and the Philippines (120°E, 15°N). Misfits in both the Earthbyte and Tomopac models occur west of the Kuril Islands in the Pacific that are of the order of 0.5–

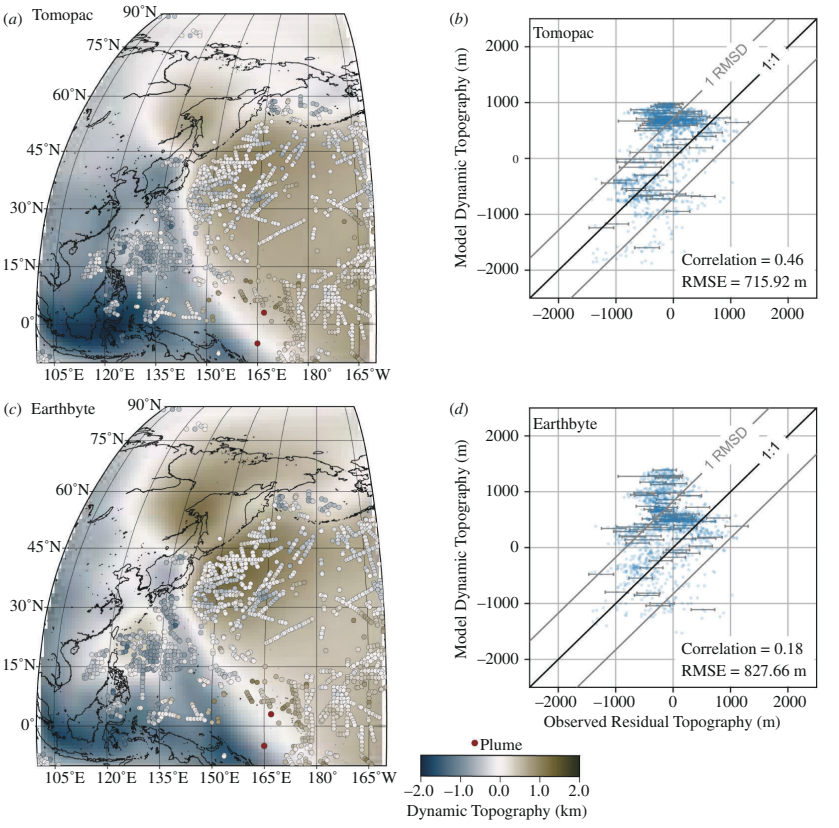

Figure 9. Maps of NE Asia showing modelled dynamic topography from (*a*) Tomopac and (*c*) Earthbyte for preferred viscosity case 06. Background colours show the magnitude of modelled dynamic topography. The points show spot measurements of observed residual topography from Holdt *et al.* [6] that are also colour-coded by dynamic topography magnitude. Associated cross-plots (*b, d*) show a comparison of modelled dynamic topography and observed residual topography from Holdt *et al.* [6] for the two mantle models. The comparisons are made within the region shown by grey dashed lines in figure 8*c* where the dynamic topography predictions show significant contrasts. Warmer colours in (*a*) and (*c*) show dynamic uplift and cool colours show dynamic subsidence. Red dots show plumes from the global catalogue of Nolet *et al.* [13]. Error bars are plotted at every 20 points. Tomopac produces a significantly better match (higher correlation, lower root mean square error (RMSE)) relative to Earthbyte in this region.

1 km (figure 9*a,c*). We plot a cross section of the model predicted dynamic topography to examine the West Philippine basin in the Philippine Sea, a key region of difference between Tomopac and Earthbyte (figure 10). Overall, trends between the predicted dynamic topography of Earthbyte (figure 10*a*, grey dashes) and Tomopac (figure 10*a*, black line) are similar, but Tomopac produces a better match because it models an additional approximately 500 m of dynamic subsidence over the entire profile A-A′. This is particularly evident in the central West Philippine basin where there are significant numbers of residual topography observations (figure 10*a*). In the southern Philippine Sea, observations are sparse but the predicted dynamic topography from Tomopac shows misfits of 0.5 to 1 km and the Earthbyte predictions may be more optimal (figure 10*a*). Although our comparisons are focused on oceanic areas, we note Earthbyte and Tomopac also produce differing dynamic topography predictions under continental regions, particularly in South Korea where they differ in the order of 1 km (figure 9). These differences are not as testable but could be targeted by future studies using recently published continental residual topography observations [49].

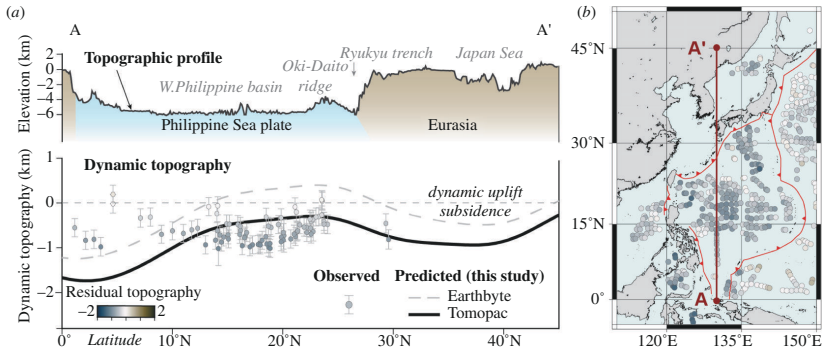

Figure 10. (*a*) Cross-section A-A′ showing the topographic profile (top panel) and associated dynamic topography (bottom panel) along eastern Eurasia and the Philippine Sea. Observed dynamic topography is shown by the colour-coded dots, which are residual depth spot measurements of Holdt *et al*. [6] projected within ± 3° longitude from the cross section. Thick lines show predicted dynamic topography (this study) from mantle models that implemented the Earthbyte and Tomopac subduction histories using our preferred radial viscosity visc06. (*b*) Location map showing cross section and colour-coded spot measurements of Holdt *et al*. [6]. The Philippine Sea shows up to 1.5 km dynamic subsidence that is more closely reproduced by modelled dynamic topography using the Tomopac subduction history.

4. Discussion

(a) Effects of deep-time subduction history on modern dynamic topography

Many previous studies have used global mantle convection models to predict modern dynamic topography [2,8,39,46,48,50] in an effort to examine the dynamics of plumes, the asthenosphere, the lithosphere and long-term sea level variations. These studies have conventionally used one family of plate reconstructions represented by our Earthbyte models. We now build upon previous analyses by directly investigating the impact of subduction history where we compare predictions of dynamic topography from two realistic plate reconstruction scenarios (Tomopac and Earthbyte) with the residual topography catalogue of Holdt *et al.* [6]. Our results allow us to argue that predicted dynamic topography is more sensitive to subduction history than viscosity at every tested spherical harmonic degree; specifically, subduction history improves correlations to observations by up to 60% whereas changes in radial viscosity improve correlations by only 30% (figure 7*a*), which is a factor of 2 lower than subduction history.

The main difference between the Tomopac and Earthbyte plate reconstructions is within the Pacific realm where Tomopac implements more intra-oceanic subduction between 160 and 50 Ma (figure 3). These regional subduction history differences have a clear influence on the modelled mantle structures (electronic supplementary material, figures S2, S3 and S8), the geoid (figure 6) and, in turn, the predicted dynamic topography (figure 8). Globally, when compared with the observed residual topography catalogue of Holdt *et al.* [6], we obtain correlations of 0.27 for Tomopac and 0.20 for Earthbyte at a spherical harmonic degree of 40 for our preferred models (figure 7*a*). These global correlations are lower than those obtained by previous studies comparing against previous estimates of present-day dynamic topography [39,46,48] where correlation values are closer to 0.4 and as high as 0.66. This is likely due to the order of magnitude improvement in available observed residual topography spot measurements from Holdt *et al.* [6], which was unavailable for these previous studies and now yields more spatial coverage for comparisons with model predictions. Also, previous studies typically use lower spherical harmonic summations [39,46,51].

With this taken into consideration, Tomopac improves the fit with observed residual topography by more than 20% for all viscosity profiles at a high spherical harmonic degree of 40 (figure 7*a*). When comparing model predictions with the longer wavelength (lower spherical harmonic degree) component of the Holdt *et al.* [6] catalogue we obtain global correlation

values for Tomopac and Earthbyte like the studies mentioned above [39,44,48], of the order of 0.5 for both degrees 3 and 10 (figure 7). At the longest wavelengths (i.e. degree 3) both Tomopac and Earthbyte show similar correlation values, 0.53 and 0.54, respectively (figure 7*b*,*e*). At higher spherical harmonic summations (i.e. degrees 1 through 10 or degrees 1 through 40) the Tomopac family of models show consistently higher correlations to observations (i.e. improvements of approx. 9 and 37%) (figure 7*c*,*d*). We attribute these improvements to the higher spherical harmonic degrees capturing more of the intermediate scale mantle structure differences between Tomopac and Earthbyte, for example, at 993 to 1941 km depths (electronic supplementary material, figure S8).

The largest changes in subduction history between Tomopac and Earthbyte occur in NE Asia (figures 9 and 10). Typically plate tectonic, geological and geodynamic studies use an Andean-style subduction framework off the coast of NE Asia [52,53]. The recent studies of Liu *et al.* [45] and Lin *et al.* [16] directly compute and compare regional differences of predicted dynamic topography in NE Asia with the observed residual topography catalogue of Hoggard *et al.* [5]. Lin *et al.* [16] found that the addition of intra-oceanic subduction increases the correlation to 0.46 compared with 0.25 and decreases the root mean square deviation (RMSD) error for predictions of modern-day topography. We perform a similar analysis using the Holdt *et al.* [6] catalogue that contains more observations by an order of magnitude and more spatial coverage. Our correlations in NE Asia remain consistent with Lin *et al.* [16]; Tomopac (the intra-oceanic case) produces a correlation of 0.46 to observed residual topography and Earthbyte (the Andean-style case) produces a correlation of 0.18 (figure 9). Specifically, the Tomopac deep-time subduction history results in approximately 500 m of dynamic subsidence in the West Philippine basin that more closely matches the regional observed residual topography (figure 10*a*). Our results continue to support intra-oceanic subduction in NE Asia during the Mesozoic and early Cenozoic and challenge plate reconstructions that only implement straightforward Andean-style subduction in NE Asia. Overall, our results suggest that any previously deep-time subduction zones that are unaccounted for will have strong impacts on predictions of dynamic topography through time and in the present day.

(b) Impact of plumes on predicting dynamic topography from mantle convection models

One well-known problem with traditional grid point metrics is the 'double penalty' problem. This occurs when the prediction of an observable is correct in magnitude, but incorrect in its location, and often results in larger RMSD errors and lower correlations [54,55]. Predictions of dynamic topography from mantle convection models are also hampered by this limitation [54,55]. For example, it is well known that geodynamic models produce plumes in the general location of actual plumes, but not in the exact geographic locations. Therefore, it is informative to characterize the potential effect of plumes in mismatches between predicted and observed ocean dynamic topography. In other words, to assess the mismatches that originate from high dynamic uplifts above plumes in the real Earth that are not reproduced by the mantle convection models.

Here, we take the Iceland plume as an example (figure 11). The Iceland plume is located near 17°W, 64°N and is associated with anomalously high observed residual topography of up to 2 km uplift (figure 11*a*). We re-examine our scatter plot of predicted dynamic topography from our preferred Tomopac model using the best-match radial viscosity profile (viscosity profile 06) against the observed residual depths [6] and filter for points within 10° of the Iceland plume (red dots in figure 11*b*). The resulting points in figure 11*b* fit with a region of obvious outliers, confirming that our preferred model underpredicts the dynamic topography associated with Iceland by 500 to 1500 m. This suggests that a more thorough removal of modelled plumes may improve the correlation between models and residual depth measurements. Alternatively, future work aiming to mitigate the double penalty problem can shift away from traditional

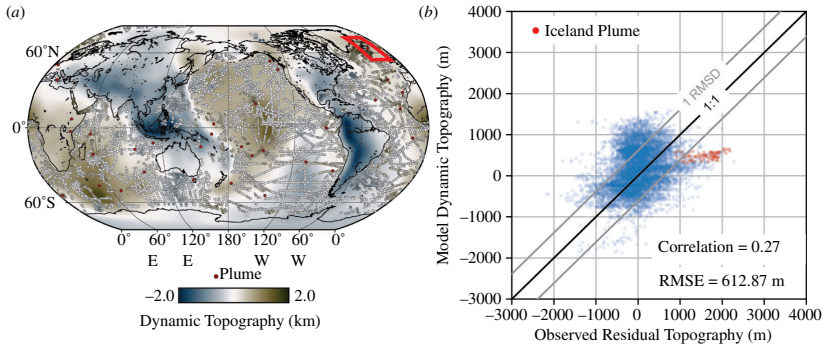

Figure 11. (*a*) Map of predicted dynamic topography for Tomopac using preferred viscosity case 06. The points show spot measurements of observed residual topography from Holdt *et al*. [6] that are also colour-coded by dynamic topography magnitude. The red box highlights the positive dynamic topography (i.e. uplift) around the Iceland plume; the spot measurements in the red box correspond to the outlier red dots in the scatter plot in (*b*). The spatial offset between the modelled Iceland plume and actual dynamic uplift creates significant misfits that skew the correlation between predicted and observed dynamic topography towards a less optimistic view. The scatter plot in (*b*) shows a comparison of modelled dynamic topography from (a) against the observed residual topography of Holdt *et al*. [6]. RMSE = root mean square error.

grid point metrics and opt for object identification methods such as those commonly used in meteorology [54–56].

(c) Regional model changes produce global perturbations

Previous research has indicated the importance of mantle convection, subduction zone geometry and slab angle for the expression of dynamic topography at both regional and global scales [2,16,39,46,57,58]. Typically, studies have imposed singular plate reconstructions (i.e. the Earthbyte model) for predicting dynamic topography or advecting seismic tomography anomalies backwards in time, which disregards deep-time anomalies [46,57]. As previously mentioned, Lin *et al*. [16] examined changes in subduction history in the circum-Pacific and examined the differences in predicted dynamic topography in comparison with the residual topography dataset from Hoggard *et al.* [5]. At the time, comparison with only a handful of observed data points was possible and no direct comparison between model predictions was made (i.e. residuals in predicted dynamic topography from two plate reconstructions). We now compare intra-oceanic subduction histories in the circum-Pacific with orders of magnitude more observed residual topography data points from Holdt *et al.* [6]. One key result from comparing models that assimilate differing plate reconstructions is summarized in figure 8*c*. In our models, the only change is related to the assimilated plate reconstruction and these reconstructions themselves only differ in the circum-Pacific from 190 to 50 Ma. Even so, these deep-time changes in subduction history have significant impacts on present-day predicted dynamic topography; for example, predicted dynamic topography between Tomopac and Earthbyte show differences of the order of half a kilometre in central Asia, India, Eastern Europe and North America (figure 8*c*) (i.e. western North America) (figures 8 and 9). More importantly, these changes in the circum-Pacific result in large-scale (up to 0.5 km) changes in predicted topography far away (more than 5000 km) from the region containing the differences in plate reconstruction. This implies that global mantle convection models should ideally be considered for regional studies of dynamic topography. Ignoring contributions from global changes in mantle convection could lead to substantial errors in regional predictions and provide misleading conclusions.

(d) Limitations: the power disparity

As mentioned in §§1a and 2c, density anomalies above a certain depth within the upper mantle are often truncated in geodynamic modelling studies to compensate for modelling limitations that include unrealistic thermal boundary layers, the compositional assumptions of models and lower Rayleigh numbers with respect to the observable Earth. Accounting for these limitations allows for more realistic magnitudes of dynamic topography with respect to observations. A recent study by Richards *et al.* [44] provides a more nuanced consideration of boundary layer compositional variations and the effect of anelasticity on seismic velocity-to-density scaling by using a calibrated parametrization for anelasticity to convert upper mantle shear wave velocities into temperature, density and viscosity. These improved images of the upper mantle structure substantially improve fits to the power spectrum of observed residual topography. When only considering the upper 400 km of their tomographic models a correlation of 0.54 with observed residual topography is obtained. Whole mantle correlations using their tomographic model also reach correlations of 0.57 with the observed residual topography from Hoggard *et al.* [5]. These results highlight the importance of improving the uppermost structure of the mantle in global mantle convection and utilizing a model resolution that allows for an appropriately defined asthenospheric model.

We examine the effects of changing this cut-off depth in figure 5. Both the Tomopac and Earthbyte models produce similar power spectra, so we focus on the illustration of the depth cut-off on the Tomopac model (figure 5). Our deep 350 km cut-off depth produces similar magnitudes of power to the observed power spectrum at lower spherical harmonic degrees (figure 5). A shallower depth cut-off allows for the inclusion of shorter wavelength density anomalies and therefore increases the power at higher spherical harmonic degrees, as expected (figure 5). While still falling short of the higher order power observed by Holdt *et al.* [6], a shallower cut-off produces a slope that is more similar to the observed data. The similarity of the slope of our results gives us confidence that the overall dynamics of the model are Earth-like, since the slope of the power spectrum of mantle density anomalies is dictated by the vigour of convection and viscosity structure, and is important for determining the large-scale variations in viscosity stratification [59]. Shallow buoyancy anomalies may be somewhat limited by our model resolution and may account for the overprediction of dynamic uplift in the Pacific. Future computational methods (i.e. TerraNeo) [60] may reduce the need for a depth cut-off by allowing for higher resolution whole-mantle convection models that include more Earth-like lithospheric and asthenospheric rheology and shorter wavelength density anomalies.

5. Conclusions

We examine the role of deep-time (i.e. back to the Jurassic) subduction history in modelling present-day dynamic topography by considering alternative plate reconstructions assimilated in mantle convection models. The overall correlations between our predicted dynamic topography and observed residual topography of Holdt *et al.* [6] are between approximately 0.50 and approximately 0.20, with higher correlations at lower spherical (up to degree 3) harmonic degrees but remain of the same order as previous studies. Our results show that dynamic topography models are up to 30% more sensitive to changes in subduction history than the choice of radial viscosity. Here, the implementation of an enhanced subduction history within the circum-Pacific that includes more intra-oceanic subduction (i.e. Tomopac) produces consistently higher correlations with the geoid (more than 20%) at all spherical harmonic degrees relative to the Earthbyte reference model. For Earth-like wavelengths of dynamic topography (i.e. degree 40), plate reconstructions that include Pacific intra-oceanic subduction universally produce higher correlations to the Holdt *et al.* [6] catalogue and improve the fit by

up to 37%. Regionally, in NE Asia where the plate reconstructions are most disparate, the family of models that includes intra-oceanic subduction shows substantially higher correlations (0.46 versus 0.18) to observed residual topography. We demonstrate more explicitly than previous studies that regional deep-time changes in subduction history can have far-reaching impacts on the spatial distribution and magnitude of present-day dynamic topography; thus, it is crucial to consider global mantle convection when modelling dynamic topography within a smaller local region. Future dynamic topography studies of regions with uncertain subduction histories should seek to implement a diversity of plate reconstructions to fully investigate the possible dynamic topography outcomes.

Data accessibility. The data used in this study can be found in the University of Arizona ReDATA repository [61]. GPlates software [62] from EarthByte Group was used to develop plate reconstructions. Paraview software [63] was used to visualize and analyse the mantle convection model.

Supplementary material is available online [64].

Declaration of AI use. We have not used AI-assisted technologies in creating this article.

Authors' contributions. C.M.C.: data curation, formal analysis, investigation, methodology, software, visualization, writing—original draft, writing—review and editing; J.W.: conceptualization, supervision, writing—review and editing; L.C.: conceptualization, software, supervision; Y.-A.L.: data curation; Y.Z.: supervision, writing—review and editing.

All authors gave final approval for publication and agreed to be held accountable for the work performed therein.

Conflict of interest declaration. We declare we have no competing interests.

Funding. Chris Calvelage, Jonny Wu and Yi-An Lin were supported by the US National Science Foundation EAR-1848327 and EAR-2422671. Chris Calvelage, Yi -An Lin, Jonny Wu and Lorenzo Colli acknowledge funding from the State of Texas Governor's University Research Initiative (GURI), the use of the UH Sabine and Carya Clusters, advanced support from the UH Research Computing Data Core and Gocad software educational licences from Emerson Paradigm.

Acknowledgements. We thank Megan Holdt, Yi-Wei Chen and Karol Czarnota for their helpful discussions. The Editor and three anonymous reviewers improved the paper.

References

1. Braun J. 2010 The many surface expressions of mantle dynamics. *Nat. Geosci.* **3**, 825–833. (doi:10.1038/ngeo1020)
2. Flament N, Gurnis M, Müller RD. 2013 A review of observations and models of dynamic topography. *Lithosphere* **5**, 189–210. (doi:10.1130/L245.1)
3. Winterbourne J, White N, Crosby A. 2014 Accurate measurements of residual topography from the oceanic realm. *Tectonics* **33**, 982–1015. (doi:10.1002/2013TC003372)
4. Hoggard MJ, White N, Al-Attar D. 2016 Global dynamic topography observations reveal limited influence of large-scale mantle flow. *Nat. Geosci.* **9**, 456–463. (doi:10.1038/ngeo2709)
5. Hoggard MJ, Winterbourne J, Czarnota K, White N. 2017 Oceanic residual depth measurements, the plate cooling model, and global dynamic topography. *J. Geophys. Res. Sol. Ear.* **122**, 2328–2372. (doi:10.1002/2016JB013457)
6. Holdt MC, White NJ, Stephenson SN, Conway-Jones BW. 2022 Densely sampled global dynamic topographic observations and their significance. *J. Geophys. Res. Sol. Ear.* **127**, e2022JB024391. (doi:10.1029/2022JB024391)
7. Miller KG *et al.* 2005 The phanerozoic record of global sea-level change. *Science* **310**, 1293–1298. (doi:10.1126/science.1116412)
8. Moucha R, Forte AM, Mitrovica JX, Rowley DB, Quéré S, Simmons NA, Grand SP. 2008 Dynamic topography and long-term sea-level variations: there is no such thing as a stable continental platform. *Earth Planet. Sci. Lett.* **271**, 101–108. (doi:10.1016/j.epsl.2008.03.056)
9. Mitrovica JX, Austermann J, Coulson S, Creveling JR, Hoggard MJ, Jarvis GT, Richards FD. 2020 Dynamic topography and ice age Paleoclimate. *Annu. Rev. Earth Planet. Sci.* **48**, 585–621. (doi:10.1146/annurev-earth-082517-010225)

10. Bahadori A *et al.* 2022 Coupled influence of tectonics, climate, and surface processes on landscape evolution in southwestern North America. *Nat. Commun.* **13**, 4437. (doi:10.1038/s41467-022-31903-2)
11. Loughney KM, Badgley C, Bahadori A, Holt WE, Rasbury ET. 2021 Tectonic influence on cenozoic mammal richness and sedimentation history of the basin and range, western North America. *Sci. Adv.* **7**, eabh4470. (doi:10.1126/sciadv.abh4470)
12. McKenzie DP. 1967 Some remarks on heat flow and gravity anomalies. *J. Geophys. Res.* **72**, 6261–6273. (doi:10.1029/JZ072i024p06261)
13. Nolet G, Karato SI, Montelli R. 2006 Plume fluxes from seismic tomography. *Earth Planet. Sci. Lett.* **248**, 685–699. (doi:10.1016/j.epsl.2006.06.011)
14. Conrad CP, Husson L. 2009 Influence of dynamic topography on sea level and its rate of change. *Lithosphere* **1**, 110–120. (doi:10.1130/L32.1)
15. Lin YA, Colli L, Wu J, Schuberth BSA. 2020 Where are the Proto-South China sea slabs? SE Asian plate tectonics and mantle flow history from global mantle convection modeling. *J. Geophys. Res. Solid Earth* **125**, e2020JB019758. (doi:10.1029/2020JB019758)
16. Lin YA, Colli L, Wu J. 2022 NW Pacific-Panthalassa intra-oceanic subduction during Mesozoic times from mantle convection and geoid models. *Geochem. Geophys. Geosyst.* **23**, e2022GC010514. (doi:10.1029/2022GC010514)
17. Menard HW. 1973 Depth anomalies and the bobbing motion of drifting islands. *J. Geophys. Res.* **78**, 5128–5137. (doi:10.1029/JB078i023p05128)
18. Colli L, Bunge HP, Oeser J. 2020 Impact of model inconsistencies on reconstructions of past mantle flow obtained using the adjoint method. *Geophys. J. Int.* **221**, 617–639. (doi:10.1093/gji/ggaa023)
19. Bunge HP, Hagelberg CR, Travis BJ. 2003 Mantle circulation models with variational data assimilation: inferring past mantle flow and structure from plate motion histories and seismic tomography. *Geophys. J. Int.* **152**, 280–301. (doi:10.1046/j.1365-246X.2003.01823.x)
20. Colli L, Ghelichkhan S, Bunge HP, Oeser J. 2018 Retrodictions of mid paleogene mantle flow and dynamic topography in the Atlantic region from compressible high resolution adjoint mantle convection models: sensitivity to deep mantle viscosity and tomographic input model. *Gondwana Res.* **53**, 252–272. (doi:10.1016/j.gr.2017.04.027)
21. Matthews KJ, Maloney KT, Zahirovic S, Williams SE, Seton M, Müller RD. 2016 Global plate boundary evolution and kinematics since the late Paleozoic. *Glob. Planet. Change* **146**, 226–250. (doi:10.1016/j.gloplacha.2016.10.002)
22. Wu J, Lin YA, Colli L, Chen YW, Fuston S, Wu TJJ. 2022 First views from assimilation of a new 'tomographic' circum-pacific plate reconstruction into mantle circulation models. EGU22-10560. (doi:10.5194/egusphere-egu22-10560)
23. Ricard Y, Richards M, Lithgow-Bertelloni C, Le Stunff Y. 1993 A geodynamic model of mantle density heterogeneity. *J. Geophys. Res.* **98**, 21895–21909. (doi:10.1029/93JB02216)
24. Steinberger B, Holme R. 2008 Mantle flow models with core-mantle boundary constraints and chemical heterogeneities in the lowermost mantle. *J. Geophys. Res. Solid Earth* **113**. (doi:10.1029/2007JB005080)
25. Nerlich R, Colli L, Ghelichkhan S, Schuberth B, Bunge HP. 2016 Constraining central neotethys ocean reconstructions with mantle convection models. *Geophys. Res. Lett.* **43**, 9595–9603. (doi:10.1002/2016GL070524)
26. Steinberger B, Calderwood AR. 2006 Models of large-scale viscous flow in the Earth's mantle with constraints from mineral physics and surface observations. *Geophys. J. Int.* **167**, 1461–1481. (doi:10.1111/j.1365-246X.2006.03131.x)
27. Calvelage CM, Colli L, Wu J, Lin YA, Zheng Y, Rahimzadeh Bajgiran M. Effects of subduction history on true polar Wander driven by perturbations of Earth's inertial moment from mantle convection. *Proc. R. Soc. A* In press.
28. Bunge HP, Richards MA, Lithgow-Bertelloni C, Baumgardner JR, Grand SP, Romanowicz BA. 1998 Time scales and heterogeneous structure in geodynamic earth models. *Science* **280**, 91–95. (doi:10.1126/science.280.5360.91)
29. Jarvis GT, Mckenzie DP. 1980 Convection in a compressible fluid with infinite prandtl number. *J. Fluid Mech.* **96**, 515–583. (doi:10.1017/S002211208000225X)

30. Chust TC, Steinle-Neumann G, Dolejš D, Schuberth BSA, Bunge H -P. 2017 MMA-EoS: a computational framework for mineralogical thermodynamics. *J. Geophys. Res.* **122**, 9881–9920. (doi:10.1002/2017JB014501)
31. Calvelage CM, Wu J, Colli L, Lin Y-A, Y Zheng. Dataset: Linking deep-time subduction history to modern day expressions of dynamic topography. In press. (doi:10.25422/azu.data.25527049.v)
32. Sager WW, Kim J, Klaus A, Nakanishi M, Khankishieva LM. 1999 Bathymetry of Shatsky Rise, northwest Pacific Ocean: implications for ocean plateau development at a triple junction. *J. Geophys. Res.* **104**, 7557–7576. (doi:10.1029/1998JB900009)
33. Ueda H, Miyashita S. 2005 Tectonic accretion of a subducted intraoceanic remnant arc in Cretaceous Hokkaido, Japan, and implications for evolution of the Pacific northwest. *Island Arc* **14**, 582–598. (doi:10.1111/j.1440-1738.2005.00486.x)
34. Wu J, Lin YA, Flament N, Wu JJ, Liu Y. 2022 Northwest Pacific-Izanagi plate tectonics since Cretaceous times from western Pacific mantle structure. *Earth Planet. Sci. Lett.* **583**, 117445. (doi:10.1016/j.epsl.2022.117445)
35. Vaes B, van Hinsbergen DJJ, Boschman LM. 2019 Reconstruction of subduction and back-arc spreading in the NW Pacific and Aleutian basin: clues to causes of cretaceous and eocene plate reorganizations. *Tectonics* **38**, 1367–1413. (doi:10.1029/2018TC005164)
36. Domeier M, Shephard GE, Jakob J, Gaina C, Doubrovine PV, Torsvik TH. 2017 Intraoceanic subduction spanned the Pacific in the Late Cretaceous-Paleocene. *Sci. Adv.* **3**, eaao2303. (doi:10.1126/sciadv.aao2303)
37. Fuston S, Colli L, press WJI. Cretaceous collision reconciles western North American tectonics with deep mantle slabs. GSA Memoir: Geological Society of America, in review. In press.
38. Chen YW, Wu J, Suppe J. 2019 Southward propagation of Nazca subduction along the Andes. *Nature* **565**, 441–447. (doi:10.1038/s41586-018-0860-1)
39. Flament N. 2019 Present-day dynamic topography and lower-mantle structure from palaeogeographically constrained mantle flow models. *Geophys. J. Int.* **216**, 2158–2182. (doi:10.1093/gji/ggy526)
40. Schaber K, Bunge H -P., Schuberth BSA, Malservisi R, Horbach A. 2009 Stability of the rotation axis in high-resolution mantle circulation models: weak polar wander despite strong core heating. *Geochem. Geophys. Geosyst.* **10**. (doi:10.1029/2009GC002541)
41. Richards MA, Hager BH. 1984 Geoid anomalies in a dynamic earth. *J. Geophys. Res.* **89**, 5987–6002. (doi:10.1029/JB089iB07p05987)
42. Thoraval C, Richards MA. 1997 The geoid constraint in global geodynamics: viscosity structure, mantle heterogeneity models and boundary conditions. *Geophys. J. Int.* **131**, 1–8. (doi:10.1111/j.1365-246X.1997.tb00591.x)
43. Kennett BLN, Engdahl ER, Buland R. 1995 Constraints on seismic velocities in the Earth from traveltimes. *Geophys. J. Int.* **122**, 108–124. (doi:10.1111/j.1365-246X.1995.tb03540.x)
44. Richards FD, Hoggard MJ, White N, Ghelichkhan S. 2020 Quantifying the relationship between short-wavelength dynamic topography and thermomechanical structure of the upper mantle using calibrated parameterization of anelasticity. *J. Geophys. Res.* **125**, e2019JB019062. (doi:10.1029/2019JB019062)
45. Liu S, Ma P, Zhang B, Gurnis M. 2021 The horizontal slab beneath East Asia and its subdued surface dynamic response. *J. Geophys. Res.* **126**, e2020JB021156. (doi:10.1029/2020JB021156)
46. Straume EO, Steinberger B, Becker TW, Faccenna C. 2024 Impact of mantle convection and dynamic topography on the Cenozoic paleogeography of Central Eurasia and the West Siberian Seaway. *Earth Planet. Sci. Lett.* **630**, 118615. (doi:10.1016/j.epsl.2024.118615)
47. Bodur ÖF, Rey PF. 2019 The impact of rheological uncertainty on dynamic topography predictions. *Solid Earth* **10**, 2167–2178. (doi:10.5194/se-10-2167-2019)
48. Steinberger B. 2016 Topography caused by mantle density variations: observation-based estimates and models derived from tomography and lithosphere thickness. *Geophys. J. Int.* **205**, 604–621. (doi:10.1093/gji/ggw040)
49. Stephenson SN, Hoggard MJ, Holdt MC, White N. 2024 Continental residual topography extracted from global analysis of crustal structure. *J. Geophys. Res.* **129**, e2023JB026735. (doi:10.1029/2023JB026735)

50. Moucha R, Forte AM, Rowley DB, Mitrovica JX, Simmons NA, Grand SP. 2009 Deep mantle forces and the uplift of the Colorado Plateau. *Geophys. Res. Lett.* **36**. (doi:10.1029/2009GL039778)
51. Steinberger B. 2007 Effects of latent heat release at phase boundaries on flow in the Earth's mantle, phase boundary topography and dynamic topography at the earth's surface. *Phys. Earth. Planet. Interiors* **164**, 2–20. (doi:10.1016/j.pepi.2007.04.021)
52. Cao X, Flament N, Müller D, Li S. 2018 The dynamic topography of eastern China since the latest Jurassic period. *Tectonics* **37**, 1274–1291. (doi:10.1029/2017TC004830)
53. Müller RD *et al.* 2019 A global plate model including lithospheric deformation along major rifts and orogens since the Triassic. *Tectonics* **38**, 1884–1907. (doi:10.1029/2018TC005462)
54. Taiwo A, Bunge HP, Schuberth BSA, Colli L, Vilacis B. 2023 Robust global mantle flow trajectories and their validation via dynamic topography histories. *Geophys. J. Int.* **234**, 2160–2179. (doi:10.1093/gji/ggad188)
55. Taiwo A, Bunge HP, Craig G. 2024 A meteorology approach to assess mantle flow induced dynamic topography using object-based image processing methods. *Phys. Earth. Planet. Interiors.* **351**, 107195. (doi:10.1016/j.pepi.2024.107195)
56. Davis CA, Brown BG, Bullock R, Halley-Gotway J. 2009 The method for object-based diagnostic evaluation (MODE) applied to numerical forecasts from the 2005 NSSL/SPC spring program. *Weather. Forecast.* **24**, 1252–1267. (doi:10.1175/2009WAF2222241.1)
57. Flament N, Gurnis M, Müller RD, Bower DJ, Husson L. 2015 Influence of subduction history on South American topography. *Earth Planet. Sci. Lett.* **430**, 9–18. (doi:10.1016/j.epsl.2015.08.006)
58. Rubey M, Brune S, Heine C, Davies DR, Williams SE, Müller RD. 2017 Global patterns in Earth's dynamic topography since the Jurassic: the role of subducted slabs. *Solid Earth* **8**, 899–919. (doi:10.5194/se-8-899-2017)
59. Čížková H, Čadek O, Yuen DA, Zhou H. 1996 Slope of the geoid spectrum and constraints on mantle viscosity stratification. *Geophys. Res. Lett.* **23**, 3063–3066. (doi:10.1029/96GL02257)
60. D'Ascoli E, Brown H, Kohl N, Mohr M, Bunge HP. 2023 TerraNeo: ongoing development of a scalable mantle convection code for exascale computing. EGU-4326. (doi:10.5194/egusphere-egu23-4326)
61. Calvelage CM, Wu J, Colli L, Lin YA, Zheng Y. 2024 Data from: Linking deep-time subduction history to modern day expressions of dynamic topography. University of Arizona Research Data Repository. (doi:.org/10.25422/azu.data.25527049)
62. Müller RD et al. 2018 GPlates: Building a Virtual Earth Through Deep Time. *Geochem. Geophys. Geosyst.* **19**, 2243–2261. (doi:10.1029/2018GC007584)
63. Ahrens J, Geveci B, Law C, Hansen C, Johnson C. 2005 A review: an end-user tool for large data visualization. In The visualization handbook, p. 50038. Computer Science.
64. Calvelage C, Wu J, Colli L, Lin YA, Zheng Y. 2024 Data from: Linking deep-time subduction history to modern day expressions of dynamic topography. Figshare. (doi:10.6084/m9.figshare.c.7458425)